Determination of the long-range potential and dissociation energy of the $1\,^3\Delta_g$ state of Na_2

Bing Ji[a),b)] and Chin-Chun Tsai[c)]
Department of Physics and Institute of Materials Science, University of Connecticut, 2152 Hillside Road, U-46, Storrs, Connecticut 06269

Li Li
Department of Modern Applied Physics, Tsinghua University, Beijing 100084, China

Thou-Jen Whang
Department of Chemistry, National Cheng Kung University, Tainan 70101, Taiwan, China

A. Marjatta Lyyra
Department of Physics, Barton Hall, Temple University, Philadelphia, Pennsylvania 19122

He Wang, John T. Bahns, and William C. Stwalley[d)]
Department of Physics and Institute of Materials Science, University of Connecticut, 2152 Hillside Road, U-46, Storrs, Connecticut 06269

Robert J. LeRoy
Guelph-Waterloo Center for Graduate Work in Chemistry, University of Waterloo, Waterloo, Ontario, N2L 3G1 Canada

(Received 6 June 1995; accepted 26 July 1995)

The $1\,^3\Delta_g$ state of Na_2 has been studied extensively by both filtered fluorescence and ionization detection and analyzed by both Dunham-type expansion and near-dissociation expansion (NDE) models in the analysis. Our observations have covered 99.998% of the potential well depth with the outermost Rydberg–Klein–Rees (RKR) turning point at 28.02 Å. NDE analysis gives T_e=28 032.468 (±0.021) cm^{-1}, D_e=7162.436 (±0.021) cm^{-1}, and R_e=3.463 81 (±0.000 28) Å. Significant long-range behavior in the near dissociation levels has been observed. Fitting of the RKR turning points gives the long-range coefficients C_5=1.388 (±0.031)×10^6 cm^{-1} $Å^5$ and C_6=0.4008 (±0.0046)×10^8 cm^{-1} $Å^6$. These newly observed results show reasonable agreement with recent theoretical calculations.

I. INTRODUCTION

Several rovibrational levels (v=3–7, 35, 38, 39, 50–55, 57, 58, and 62) of the $1\,^3\Delta_g$ state of Na_2 have been experimentally observed by the high resolution cw perturbation facilitated optical–optical double resonance technique (PFOODR).[1–4] Along with other Rydberg states in Na_2, the fine–hyperfine structure of the $1\,^3\Delta_g$ state has been characterized as Hund's case ($b_{\beta S}$) for those observed levels.[2] Reference 4 also reported $4\,^1\Sigma_g^+ \sim 2\,^3\Pi_g \sim 1\,^3\Delta_g$ triple perturbation analysis for levels $(v_\Sigma, v_\Pi, v_\Delta)$=(6,2,7) and (7,3,8). *Ab initio* calculations[5–8] have corroborated these experimental results. One interesting feature emerging from the most recent theoretical studies (both *ab initio*[7,8] and long-range analysis[9,10]) is that the $1\,^3\Delta_g$ state of Na_2 has a purely attractive potential at long range. Since the $1\,^3\Delta_g$ state is a Rydberg state that dissociates into $Na(3s)+Na(3d)$ asymptotes and is the lowest one of its symmetry, a detailed experimental study of its long-range potential cannot only reveal valuable insights into the long-range interactions in molecular Rydberg states as well as ultracold collisions involving excited state atoms, but also provide a stringent test of the recent high quality theoretical calculations.

As pointed out in Ref. 1, PFOODR spectroscopy is one of the most fruitful techniques in the investigation of excited triplet gerade states. In this technique a PUMP laser is used to transfer molecular population from the ground singlet ($X\,^1\Sigma_g^+$) levels into the singlet ($A\,^1\Sigma_u^+$)~triplet ($b\,^3\Pi_u$) mixed ungerade levels which act as windows for the PROBE laser to access excited gerade triplet states. When high resolution cw lasers are used, one can resolve the fine–hyperfine structures which provide important information about electronic interactions unavailable from singlet spectra alone. It is therefore a rewarding venture to extend the PFOODR spectroscopy of the $1\,^3\Delta_g$ state of Na_2 over the entire potential well depth, especially the highest vibrational levels near the dissociation limit so that the long-range potential of the $1\,^3\Delta_g$ state can be constructed accurately and the associated molecular properties at long range can be studied quantitatively. In addition, direct observation of the near dissociation rovibrational levels enables accurate determination of the dissociation energy through long-range analysis without large extrapolations. The importance of such direct experimental observation of rovibration levels near dissociation limit has been summarized by Tellinghuisen.[11]

To achieve this goal, several challenges must first be met: (i) direct observation of both the high-lying near dissociation rovibrational levels and the low-lying near equilib-

[a)]Also at Department of Physics and Astronomy, University of Iowa, Iowa City, Iowa 52242.
[b)]Present address: Department of Chemistry, Massachusetts Institute of Technology, Cambridge, Massachusetts 02139.
[c)]Present address: Department of Physics, University of Texas at Austin, Austin, Texas 78712.
[d)]Also at Department of Chemistry. To whom correspondence should be sent.

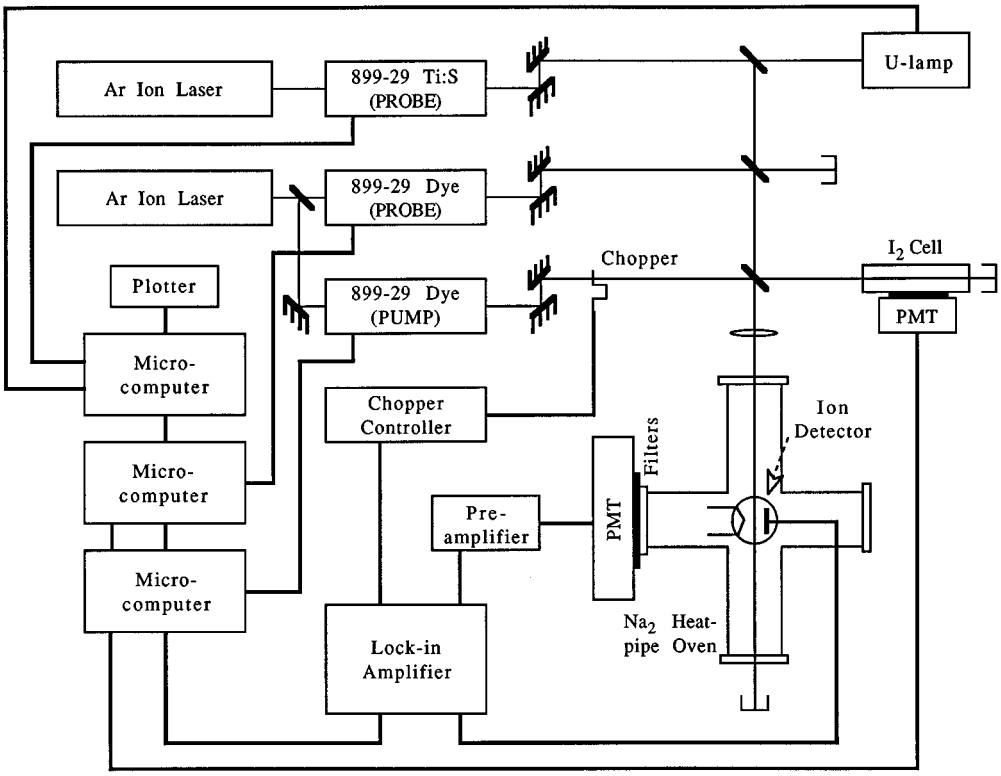

FIG. 1. Experimental setup.

rium rovibrational levels, which are vital in the determination of the dissociation energy and the long-range potential; and (ii) analysis of the spectral data over a wide range of vibrational levels from which the long-range potential can be constructed. In this work, (i) is achieved by using a high sensitivity cylindrically shielded ionization detector[12] and a cw Ti:sapphire ring laser; and (ii) is addressed by applying the near dissociation expansion (NDE) theory.[11,13,14] The results and analysis will be reported in detail in this paper.

II. EXPERIMENT

Figure 1 shows the schematics of the experimental set up. The PUMP laser was a CR 899-29 (Coherent Inc.) ring dye laser operated with DCM or Rhodamine 6G dyes and pumped by an Innova 200-25 (Coherent Inc.) argon ion laser. Depending on the transition frequencies, the PROBE laser was either a CR 899-29 Ti:sapphire ring laser operated with short wavelength intracavity optics and pumped by a CR-18 (Coherent Inc.) argon ion laser, or a CR 899-29 ring dye laser operated with rhodamine 6G or rhodamine 110 dyes and pumped by the Innova 200-25 argon ion laser. Both the PUMP and the PROBE lasers were cw high resolution lasers (linewidth 500 kHz) and their frequencies were calibrated either with an iodine cell for the dye lasers or a uranium hollow cathode lamp for the Ti:sapphire laser. The PUMP and PROBE laser beams propagated collinearly in the same direction (i.e., the copropagating geometry) into the sodium heatpipe oven. The sodium heatpipe was operated at about 630 K and with about 0.1 Torr argon as buffer gas.

Two different kinds of detection schemes were used in this investigation. At first, a filtered photomultiplier tube (PMT) as described in Refs. 1–4 was used to monitor the UV/violet fluorescence from the excited triplet states. While this method was used in generating a vast amount of successful OODR spectra in the literature, its sensitivity was not high enough to observe the extremely weak PROBE transitions (Franck–Condon factor $<10^{-3}$) into $v>84$ levels in the $1\,^3\Delta_g$ state. More recently, a cylindrically shielded ionization detector[12] had demonstrated its superior sensitivity to the conventional filtered PMT method in the OODR spectra of the singlet states of Na_2.[15–21] In this work, near dissociation levels ($v=85$–95) of the $1\,^3\Delta_g$ state were observed for the first time using this novel ionization detector.

In both detection schemes, the PUMP laser was modulated by a mechanical chopper and a lock-in amplifier was used to selectively amplify the OODR signals. For the very weak signals, several different ground state ($X\,^1\Sigma_g^+$) levels were chosen for PUMP transitions to the same intermediate levels. In this way, the desired OODR signals were confirmed and spurious signals from coincidental pumping were eliminated.

In order to enhance signal-to-noise ratio for the weakest transitions into the last few vibrational levels just below the dissociation limit, signal averages from repeated slow scans had to be taken. In some cases, a 10 GHz scan took as long as an hour to complete. Figure 2 shows the data from one of these scans.

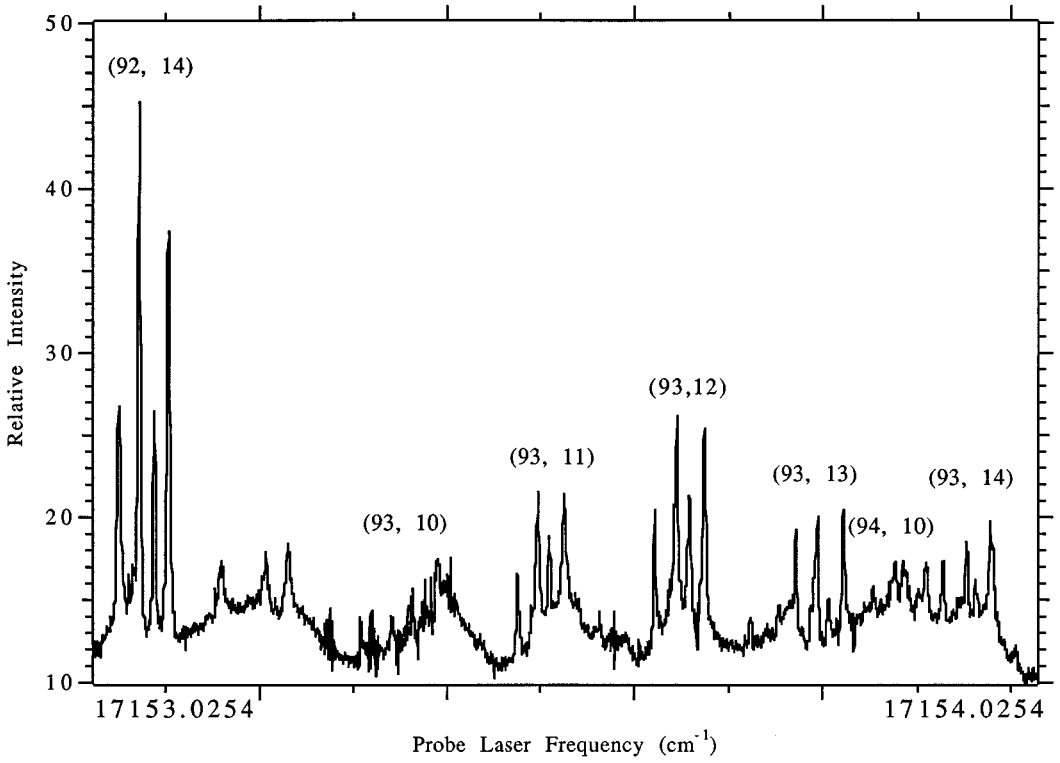

FIG. 2. PROBE laser spectrum for high lying vibrational levels of the $1\,^3\Delta_g$ state of Na_2. The numbers in the parentheses designate the vibrational and rotational quantum numbers v and N, respectively, of each assigned transition. The intermediate level populated by the PUMP laser is $b\,^3\Pi_{1u}$ ($v'=32$, $J'=12$), which is 18 040.9510 cm^{-1} above the minimum of the $X\,^1\Sigma_g^+$ state of Na_2 (Refs. 1–4).

III. RESULTS

For all the data taken in this study, the intermediate levels are the $\Omega=1$ component of the $b\,^3\Pi_u$ state. Since the hyperfine splitting of the $\Omega=1$ component of the $b\,^3\Pi_u$ state is negligible,[22] the typical Hund's case ($b_{\beta S}$) fine–hyperfine multiplet structure as shown in Fig. 2 is mainly from the $1\,^3\Delta_g$ state.[1,2] This is indeed the case for all the data observed, ranging from $v=0$ to the highest vibrational level $v=95$. Selection rules give five allowed PROBE branches from each intermediate level, viz., $N=J'$, $J'\pm1$, and $J'\pm2$. Usually the $N=J'\pm2$ branches are weaker than the others. For every recorded PROBE transition, the ''center of gravity'' average (i.e., average of the fine–hyperfine multiplet frequencies weighted by their respective peak intensities) over all the resolved fine–hyperfine components is taken as the line center which gives the term value for the assigned rovibrational level.

The term values obtained from the two different detection schemes are combined with those published results in the literature[1–4] for the analysis to follow. Altogether, the total data set is comprised of 501 distinct rovibrational levels covering 57 vibrational bands. In particular, levels both near the equilibrium and near the dissociation limit have been extensively searched for in this work to ensure the quality of the long-range analysis to follow. Figure 3 shows the data distribution with various sources identified. Since PFOODR must take the singlet ($A\,^1\Sigma_u^+$)~triplet ($b\,^3\Pi_u$) mixed levels as the intermediate levels, we are not at liberty to choose any rotational quantum number in the PROBE step as we wish. On the other hand, the vibrational levels in the data set span across the entire potential well depth from $v=0$ to $v=95$. It is not surprising that this data set presents an enticing albeit challenging task for the analysis.

Since the term values of the intermediate levels have all been accurately determined in previous studies, the term values of the $1\,^3\Delta_g$ state can be unambiguously calculated and referred to the minimum of the ground $X\,^1\Sigma_g^+$ state potential well. This allowed us to focus the analysis on the rovibrational level energies of the $1\,^3\Delta_g$ state instead of on the transition frequencies between the two states as in some cases.[11] In the calculation of all the term values of the $1\,^3\Delta_g$ levels, the dissociation energy $D_e(X)$ of the ground $X\,^1\Sigma_g^+$ state of Na_2 is taken as 6022.03 ± 0.03 cm^{-1} from the most recent and accurate work[23,24] and the second-order correction[25] of $Y_{00}''^{(2)} = -0.0315$ cm^{-1} of the ground $X\,^1\Sigma_g^+$ state has also been taken into account.

IV. DATA REPRESENTATION AND POTENTIAL INVERSION

A. Summary of some commonly used algorithms

1. Introduction

Data representation and potential inversion have been the central themes in the spectroscopy of diatomic molecules.[25] While these two procedures are intrinsically related to each other, and in some cases, are combined together in a single scheme [such as the inverted perturbation approach (IPA) and its variations and extensions[26–28]], it is

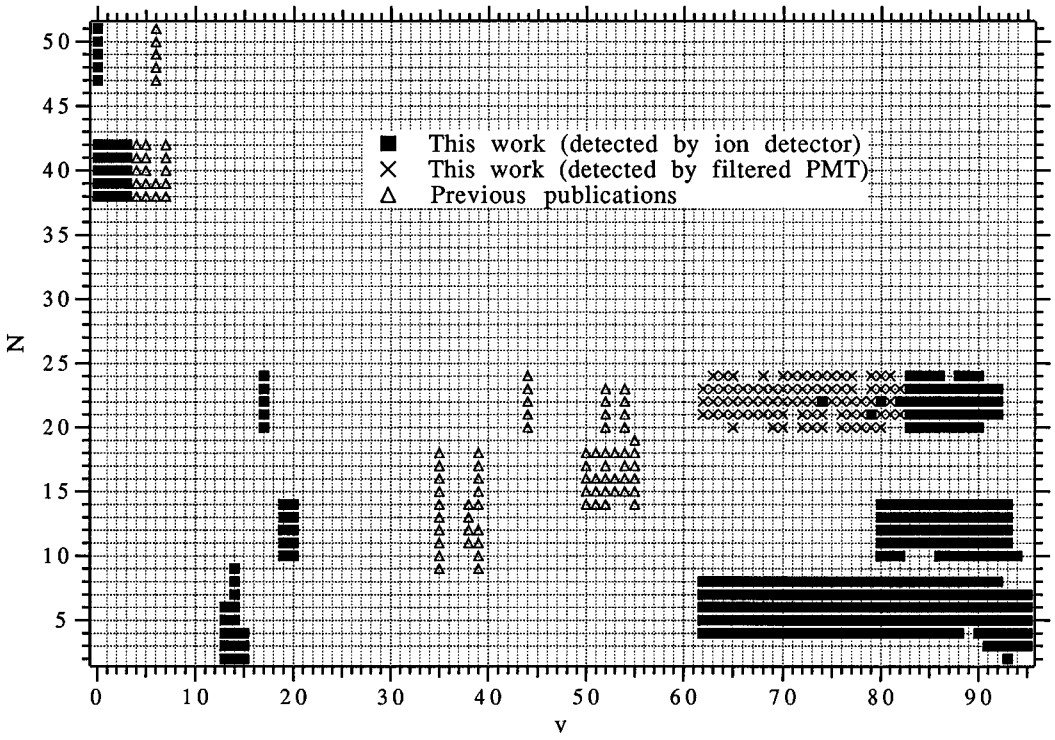

FIG. 3. The field of the (v,N) distribution of the data set employed in the analysis.

nevertheless worthwhile to distinguish them for the sake of clarity in the ensuing discussions. The goal in data representation is to obtain some compact and accurate expressions to summarize all the experimental rovibrational term values in a given electronic state. The quality of data representation can be best judged by the four criteria elucidated by Tromp and Le Roy:[13] accuracy, physics, compactness, and extrapolation ability. The problem of potential inversion is to construct a molecular potential curve based on the observed rovibrational term values in a given molecular electronic state.

There have been many excellent presentations and reviews on spectral data representation and molecular potential inversion.[13,23,27–30] The summary below is focused mainly on those methods that are pertinent to our analysis of the $1\,^3\Delta_g$ state of Na_2.

2. Dunham's procedure

In his classic work[31] Dunham derived the relations between the coefficients of the commonly used double summation expression for diatomic energy levels (often referred to as the Dunham-type expansion):

$$E(v,J)=\sum_{l=0}^{\infty}\sum_{m=0}^{\infty} Y_{lm}\left(v+\frac{1}{2}\right)^{l}[J(J+1)]^{m}, \tag{1}$$

and the coefficients of a power series expansion of the molecular potential about its equilibrium minimum:

$$V(R)=A_0\left[\frac{R-R_e}{R_e}\right]^2\left\{1+\sum_{n=1}^{\infty} a_n\left[\frac{R-R_e}{R_e}\right]^n\right\}, \tag{2}$$

where A_0 is a constant.

Using the relations given by Dunham,[31] one can obtain the potential coefficients a_n's from the rovibrational level energy coefficients Y_{lm}'s and thus at least in principle construct the potential from the experimental data. However, Beckel and Engelke[32] have pointed out that Eq. (2) has a convergence radius of R_e since the Born–Oppenheimer potential $V(R)$ has a pole at $R=0$ due to the nuclear–nuclear repulsion term. Therefore, this *potential inversion procedure* no longer converges when $R>2R_e$. Though alternatives of Eq. (2) may be employed to extend the convergence radius in the potential inversion procedure (such as the work of Ref. 33), there have been instances where Eq. (1) itself can no longer be satisfactorily employed *as an expression for spectral data representation*. In fact, despite the large amount of Y_{lm}'s that have to be used, intolerable fitting residuals arise especially when the data are fitted from the potential minimum all the way up to levels close to the dissociation limit, as is the case for the $1\,^3\Delta_g$ state of Na_2. Clearly, a new algorithm is called for.

Often times, Eq. (1) is recast into a more convenient form:

$$E(v,J)=\sum_{m=0}^{\infty} K_m(v)[J(J+1)]^m, \tag{3}$$

and

$$K_m(v)=\sum_{l=0}^{\infty} Y_{lm}\left(v+\frac{1}{2}\right)^{l}, \tag{4}$$

where $K_0(v)=G_v$ is the rotationless vibrational energy, $K_1(v)=B_v$ is the inertial rotational constant, and $K_2(v)=-D_v$, $K_3(v)=H_v$, $K_4(v)=L_v$, and $K_5(v)=M_v$, etc. are

the centrifugal distortion constants. For the $1\,^3\Delta_g$ state of Na_2, J is no longer a good quantum number in Hund's case ($b_{\beta S}$) coupling. The $[J(J+1)]$ factor in Eqs. (1) and (3) is replaced by $[N(N+1)-\Lambda^2]$ in the analysis, where N is the rotational quantum number and $\Lambda=2$ is the projection of the molecular electronic angular momentum along the internuclear axis.

3. The near-dissociation expansion theory

At sufficiently large internuclear distances, the long-range potential attains the limiting form:[29,34–36]

$$V(R)\approx D-C_n/R^n, \tag{5}$$

where D is the energy at the molecular dissociation limit and C_n is the leading long-range coefficient. Depending on the choice of the zero of the energy scale, D can be either 0 when the energy is referenced to the dissociation limit, or the molecular dissociation energy D_e when the energy is referenced to the minimum of the molecular potential. Based on Eq. (6), Le Roy and Bernstein,[34,35] Stwalley,[29,36–39] and Le Roy[40–43] derived the near dissociation limiting behaviors of the molecular properties $K_m(v)$. Specifically, they are:
for $m=0$,

$$K_0^{\infty}(v)=D-X_0(n)(v_D-v)^{2n/(n-2)}, \tag{6}$$

and, for $m\geqslant 1$,

$$K_m^{\infty}(v)=X_m(n)(v_D-v)^{[2n/(n-2)-2m]}, \tag{7}$$

where v_D is the effective vibrational index at dissociation (and generally is noninteger), and $X_m(n)=X_m(n)/[\mu^n(C_n)^2]^{1/(n-2)}$, where μ is the reduced mass of the diatomic molecule and $X_m(n)$ are known constants.[34–43]

It is apparent that the Dunham-type expansion Eq. (4) does not have the correct limiting behavior [such as the singularity of $K_m(v)$ at v_D for higher order m] and thus cannot be readily and reliably applied to vibrational levels close to dissociation. In order to incorporate the correct $K_m(v)$ behavior for *both near equilibrium and near dissociation*, Beckel and co-workers,[44–47] and Le Roy and co-workers[13,14,48–50] have developed the near dissociation expansions (NDE) as expressions for spectral data representation. In its most complete form,[13] the vibrational energy expression (GvNDE) can be summarized as

$$G_v=D-X_0(n)(v_D-v)^{2n/(n-2)}[L/M]^s, \tag{8}$$

where $[L/M]$ is a Padé approximant of order L and M:

$$\left[\frac{L}{M}\right]=\left[\frac{1+p_1z^{NDP1}+p_2z^{NDP1+1}+\cdots+p_Lz^{NDP1-1+L}}{1+q_1z^{NDQ1}+q_2z^{NDQ1+1}+\cdots+q_Mz^{NDQ1-1+M}}\right], \tag{9}$$

and s is set either at 1, which yields the "outer" Padé expansions, or at $2n/(n-2)$, which yields the "inner" Padé expansions; $z=(v_D-v)^{LPWDV}$, where $LPWDV$ is the power of the expansion variable (v_D-v); and $NDP1$ and $NDQ1$ are the leading powers in the numerator polynomial and the denominator polynomial, respectively. Together with $LPWDV$, $NDP1$, and $NDQ1$ determine how quickly the correction function $[L/M]^s$ to the limiting behavior [Eq. (6)] would "turn on."

Alternatively, exponential expansions can be used:

$$G_v=D-X_0(n)(v_D-v)^{2n/(n-2)}\exp\left[\sum_{l=1}^{L}p_i(v_D-v)^l\right]. \tag{10}$$

Other molecular properties (such as BvNDE) can also be expanded as

$$K_m(v)=K_m^{\infty}(v)\exp\left[\sum_{l=1}^{L}p_{lm}(v_D-v)^l\right]. \tag{11}$$

Equation (8) is, in a mathematical sense,[51,52] an analytical continuation of Eqs. (4) and (6) by Padé approximants. In general Eqs. (8)–(11) require nonlinear least-squares fitting. This can be conveniently done by computer codes (such as GvNDE and BvNDE).[53] Applications of the NDE algorithm in diatomic spectroscopy have demonstrated its superiority over the conventional Dunham-type expansion for large spectroscopic data sets.[11,13,14,54–57] Its capability in interpolation of missing data and extrapolation to both high v and low v for unobserved vibrational levels have been systematically tested and concluded in Refs. 11, 13, and 47. In summary, NDE extrapolation to low v is no worse than Dunham-type expansion; NDE interpolation of gaps between the observed vibrational levels (i.e., missing data) is comparable to or better than Dunham-type expansion; and NDE extrapolation to high v is *far better* than Dunham-type expansion.

4. The Rydberg–Klein–Rees method for potential inversion

The Rydberg–Klein–Rees (RKR) method is perhaps the most widely used potential inversion procedure in diatomic spectroscopy. The classical turning points $R_-(v)$ and $R_+(v)$ are calculated from the integrals:

$$R_+(v)-R_-(v)=\frac{2}{\beta}\int_{v_{\min}}^{v}\frac{dv'}{[G_v(v)-G_v(v')]^{1/2}}\equiv 2\,f, \tag{12}$$

and

$$\frac{1}{R_-(v)}-\frac{1}{R_+(v)}=\frac{1}{2\pi\beta}\int_{v_{\min}}^{v}\frac{B_v(v')dv'}{[G_v(v)-G_v(v')]^{1/2}}\equiv 2g. \tag{13}$$

Evaluation of the f and g integrals requires well-behaved continuous representation of the $G_v(v')$ and $B_v(v')$ functions. This means that the procedure of spectral data representation must first be performed properly and, furthermore, the quality of the RKR potential rests largely with the quality of the representation of the $G_v(v')$ and $B_v(v')$ functions. It should be emphasized that *any* well-behaved representation of the $G_v(v')$ and $B_v(v')$ can serve this purpose. As explained in the foregoing discussions, the Dunham-type expansion in Eq. (4), when it is valid, is just one of the many applicable function forms. Another option is to use spline interpolation of the observed G_v's and B_v's so

that the f and g integrals can be evaluated numerically. Some RKR potential curves in Na_2 have been constructed by this numerical technique when the Dunham-type expansion is no longer valid.[15–21]

When this spline interpolation approach was applied to the data set in the $1\,^3\Delta_g$ state of Na_2, however, the highest few outer turning points exhibited irregular behavior. This is because the f integral (or the well width function) approaches infinity at the dissociation limit, so that even small errors in the shape of the $G_v(v')$ function in the long-range region can give rise to large errors in the associated turning point differences.[57] Note that this singularity is different from the inner wall "wiggling" which is due to the irregular behavior of the g integral and thus cannot be remedied simply by inner wall smoothing.

The NDE algorithm given by the previous section offers physically and mathematically more reliable representation of the $G_v(v')$ and $B_v(v')$, especially when the vibrational levels are near the dissociation limit, primarily because Eqs. (8)–(11) have explicitly the correct limiting behavior in the long-range region. In our code (RKR1),[58] nonlinear least-squares fitted NDE coefficients for G_v and B_v are taken as the input to evaluate the f and g integrals.

While it is possible (and, in some cases, even desirable) to calculate the effective potential $U_J(R)$ directly by the RKR method,[24,59] it is more common to construct the rotationless RKR potential curve which is given by Eqs. (12) and (13). This requires the extraction of G_v's and B_v's from the observed rovibrational term values. Since our data set contains levels with high rotational quantum number N, or levels with very large internuclear distances, higher-order centrifugal distortion contributions cannot be neglected in the determination of the G_v's and B_v's. Unfortunately, the accessible rotational quantum numbers are limited by the intermediate window levels and there are not enough to determine unambiguously all the higher-order centrifugal distortion constants directly through least-squares fit.

To circumvent this problem, Hutson's code[60,61] (CDIST) has been adopted to calculate the centrifugal distortion constants $K_m(v)$, where $m=2$–5. An iterative procedure is taken. First, direct fit [i.e., with $m=0$–1 in Eq. (3)] to the experimental data gives the approximate G_v and B_v values from which an approximate RKR potential is constructed. With the first approximate RKR potential, the CDIST code computes the centrifugal constants which will be held fixed in the next fitting of G_v and B_v constants [i.e., with $m=0$–5 in Eq. (3), but the $m=2$–5 terms are held fixed at the computed values]. In this way, a set of "mechanically consistent" molecular constants can be obtained when the observed rotational levels are limited.[13,60,61]

B. Limited analysis by Dunham fit

Due to the inadequacies of Dunham-type expansion in data representation, only a limited set of data could be fitted by Eq. (1). Table I lists the Dunham coefficients of the $1\,^3\Delta_g$ state of Na_2 for vibrational levels $v=0$–20. Second order corrections of $Y_{00}^{(2)}=0.0016\ \mathrm{cm}^{-1}$ for the $1\,^3\Delta_g$ state and $Y_{00}''^{(2)} = -0.0315\ \mathrm{cm}^{-1}$ for the ground $X\,^1\Sigma_g^+$ state have been included in the T_e value. The dissociation energy D_e is calculated relative to the spin–orbit-averaged $\mathrm{Na}(3s)+\mathrm{Na}(3d)$ limit. [This is justified in Sec. V A.] Molecular constants from previously published work[3] and recent *ab initio* calculations[7,8] are also listed in Table I for comparison. These results show remarkable agreement. Since the current fit includes the lowest vibrational levels, the T_e and D_e values here are more accurate than those in Ref. 3. In general, the newly fitted Dunham coefficients can reproduce the observed $v=0$–20 term values to within $\pm 0.01\ \mathrm{cm}^{-1}$ or better. The exception comes with the $(v=6, N=38)$ level, where the difference between the observed and the calculated term value is $0.02\ \mathrm{cm}^{-1}$.

TABLE I. Primary molecular constants of the $1\,^3\Delta_g$ state of Na_2.

	Magnier *et al.*[a,b]	Li *et al.*[a,c]	This work[a,d]	This work[a,e]
T_e	28026	28 030.3 (0.4)[f]	28 032.4802 (0.023)[f]	28 032.468 (0.021)[f]
Y_{10}	128.7	130.01 (0.02)	129.565 6964 (0.011)	129.4635 (0.0010)
Y_{20}		−0.4806 (0.0014)	−0.451 285 0119 (0.0025)	
10^3Y_{30}		1.457 (0.040)	0.771 817 1705 (0.17)	
10^4Y_{40}		−0.2425 (0.0034)	−0.215 657 1907 (0.037)	
Y_{01}		0.1227 (0.0004)	0.122 159 1588 (0.000024)	0.122 232 (0.000 020)
10^3Y_{11}		−0.7302 (0.0066)	−0.646 275 1870 (0.0072)	
10^5Y_{21}			0.608 091 0525 (0.18)	
10^6Y_{31}			−0.457 111 3098 (0.16)	
10^8Y_{41}			0.976 790 9115 (0.48)	
10^6Y_{02}		−0.40 (0.09)	−0.426 928 4626 (0.0063)	
D_e	7039	7164.6 (0.4)[f]	7162.426 (0.023)[f]	7162.436 (0.021)[f]
R_e	3.47	3.4572[g] (0.0056)	3.464 844[g] (0.000 34)	3.463 81 (0.000 28)

[a]All quantities are in cm^{-1}, except that R_e is in Å. 1σ uncertainties are in parentheses.
[b]From Refs. 7 and 8.
[c]From Ref. 3. Note that there is a printing error in Ref. 3 for the value of Y_{10}.
[d]Based on Dunham fitting of data set $0\leqslant v\leqslant 20$, and $2\leqslant N\leqslant 51$. The figures given here are obviously not all significant. However, rounding would adversely affect the ability to reproduce accurately the energy levels.
[e]Based on NDE fitting of the entire data set $0\leqslant v\leqslant 95$, and $2\leqslant N\leqslant 51$.
[f]The second-order corrections Y_{00} for the ground $X\,^1\Sigma_g^+$ state and the $1\,^3\Delta_g$ state, respectively, have been included.
[g]Calculated from $B_e=Y_{01}=h/(8\pi^2 c\mu R_e^2)$.

C. Full analysis by NDE fit

In order to account for the contributions from the centrifugal distortion terms, the full NDE analysis adopts the iterative procedure outlined at the end of Sec. IV (A 4). The principal steps are also illustrated in Fig. 4. Convergence was achieved after three iterations. The final converged values of G_v and B_v from the least-squares fit are listed in Table II,

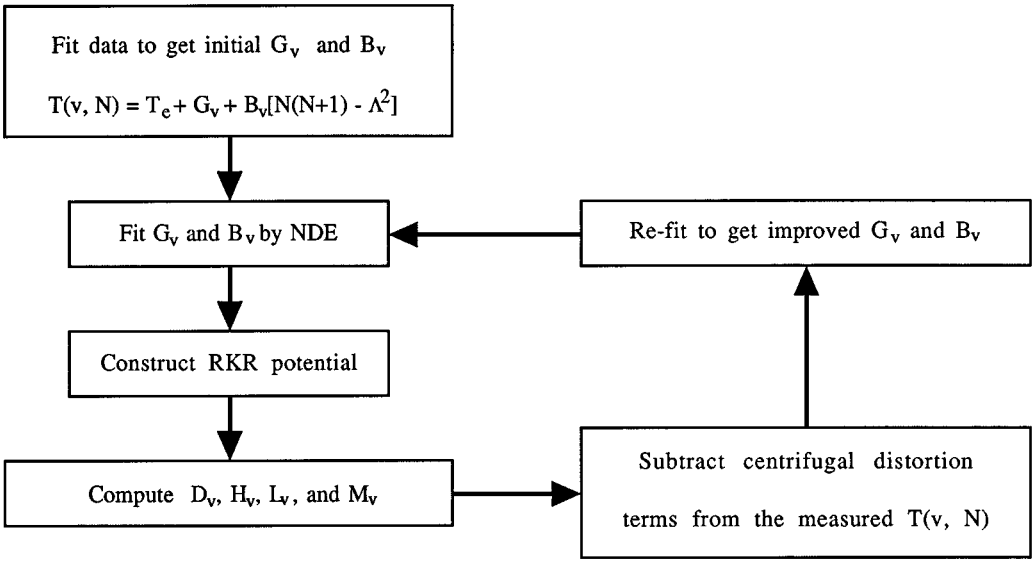

FIG. 4. The iteration procedure used in the full NDE analysis.

along with the associated 1σ deviations in the fit. These results as well as $\Delta G_{v+1/2}$ are also plotted in Fig. 5. It is apparent from the plots that the $v=39$, 83, and 84 levels are perturbed so that these data points were excluded from the final fits. Since the NDE algorithm has been shown to be able to interpolate G_v and B_v functions between the observed data points,[11,13,47] the missing intermediate vibrational levels in Fig. 3 should not have severe adverse effects on the quality of the overall potential. The data presented in Table II form the basis for the ensuing NDE and long-range analysis.

In order to carry out the NDE analysis effectively, the GvNDE[53] fit was conducted first. Recent theoretical calculations show that the $1\,^3\Delta_g$ state of Na_2 has a purely attractive potential at long range[9,10] with the leading (limiting) coefficient[9] $C_5=792\,281.769$ cm^{-1} Å^5. This theoretical C_5 value was held fixed in all the NDE fits. This is warranted because these theoretical values are of high quality and because long-range limiting behavior is not very sensitive to errors in C_n. Based on considerations of deviations from limiting behavior by higher-order C_m contributions, the leading power in the expansion is set by $LPWDV=1$, $NDP1=2$, and $NDQ1=2$. Considering the compactness, accuracy, and numerical stability against round-off errors, the [0/15] inner Padé expansion [Eq. (8) with $s=10/3$] is chosen among all the converged fits as the recommended expression to represent the entire set of observed G_v values listed in Table II. The results are listed in Table III. Note that the individual expansion parameters $\{q_i\}$ have no physical significance, so their statistical uncertainties are not reported. The residuals of the GvNDE fit (i.e., the differences between the G_v values in Table II and the calculated values from the parameters in Table III) are in general quite small. The largest residual is 0.07 cm^{-1} for the $v=6$ level. To verify the model dependence of the fitted D_e and v_D values, an ''averaging-over-models'' procedure as described in Ref. 14 is performed. For the 119 converged NDE fits based on Eqs. (8)–(10) with total number of fitting parameters between 10 and 17, the averaged v_D has a value of 96.80 ± 0.20, in excellent agreement with our recommended value $v_D=96.885\pm0.049$ in Table III.

The v_D and D_e obtained in the above GvNDE fits are held fixed together with the theoretical C_5 in the subsequent BvNDE[53] fits. The final converged and rounded results are listed in Table IV. The parameters in Table IV can reproduce the B_v values in Table II satisfactorily, with the largest difference of about 2% for the $v=92$ level.

The quality and consistency of the NDE fits is also demonstrated in Fig. 5, where G_v and B_v curves calculated from the NDE parameters in Tables III and IV overlap completely with the circles denoting the observed experimental values in Table II (except the perturbed $v=39$, 83, and 84 levels) and with the curves computed quantum mechanically by the CDIST code.

One of the powerful features of the NDE algorithm is its capability to extrapolate G_v and B_v for levels higher than the observed ones,[11,13,47] as long as part of the data set is in the long-range region. In the case of the $1\,^3\Delta_g$ state of Na_2, G_v, and B_v values of the unobserved $v=96$ level can be extrapolated based on the NDE fits in Tables III and IV. This enables us to construct physically reliable RKR potential from $v=0$ all the way up to $v=96$, even though the last bound level was not experimentally observed.

These final G_v and B_v NDE coefficients are taken as the input for the RKR1[58] program which computes the first-order RKR potential curve. Table V lists the output from the program. The final RKR potential curve of the $1\,^3\Delta_g$ state of Na_2 is plotted in Fig. 6. The inner wall ''wiggling'' occurred at $v=65$. For levels from $v=65$ up [or corresponding to inner turning point $R_-(65)\leqslant 2.3597$ Å] the inner turning points are smoothed according to[62,63]

$$V(R_-)\ (\mathrm{cm}^{-1}) = 505.7974 + 0.266\,864\,33\times10^7 \times \exp\{-2.590\,700\,19 R_-(\text{Å})\}. \qquad (14)$$

TABLE II. Least-squares fitted G_v and B_v values and their associated statistical 1σ deviations. Note: All quantities (except v) are in units of cm^{-1}. The entries listed here are the final converged values after three iterations of the steps outlined in Fig. 4 and in the text.

v	G_v	$\sigma(G_v)$	B_v	$\sigma(B_v)$
0	64.6767	0.0049	0.121 848	0.000 002
1	193.3494	0.0082	0.121 207	0.000 005
2	321.1145	0.0134	0.120 582	0.000 008
3	448.0034	0.0705	0.119 961	0.000 043
4	574.0199	0.0577	0.119 325	0.000 035
5	699.0835	0.0327	0.118 732	0.000 020
6	823.2410	0.0149	0.118 144	0.000 007
7	946.7171	0.0208	0.117 448	0.000 013
13	1668.0808	0.0077	0.113 872	0.000 346
14	1785.2265	0.0026	0.113 204	0.000 065
15	1901.4861	0.0005	0.112 711	0.000 052
17	2131.3284	0.0127	0.111 170	0.000 025
19	2357.5416	0.0009	0.109 911	0.000 006
20	2469.2905	0.0099	0.109 296	0.000 062
35	4033.6657	0.0067	0.098 911	0.000 035
38	4320.1831	0.0247	0.096 419	0.000 145
39	4413.5782	0.0119	0.095 842	0.000 054
44	4864.4835	0.0109	0.091 882	0.000 021
50	5367.7931	0.0072	0.086 513	0.000 026
51	5447.3869	0.0059	0.085 549	0.000 022
52	5525.6819	0.0093	0.084 596	0.000 024
53	5602.6463	0.0105	0.083 675	0.000 037
54	5678.3180	0.0054	0.082 545	0.000 014
55	5752.5801	0.0150	0.081 541	0.000 052
62	6231.0018	0.0016	0.073 222	0.000 007
63	6292.9527	0.0010	0.071 879	0.000 004
64	6353.1715	0.0020	0.070 479	0.000 007
65	6411.6004	0.0050	0.069 059	0.000 017
66	6468.2039	0.0014	0.067 520	0.000 005
67	6522.9041	0.0012	0.066 009	0.000 005
68	6575.6623	0.0009	0.064 383	0.000 003
69	6626.4149	0.0018	0.062 706	0.000 007
70	6675.0923	0.0015	0.060 969	0.000 005
71	6721.6455	0.0011	0.059 150	0.000 004
72	6766.0015	0.0019	0.057 265	0.000 006
73	6808.1047	0.0011	0.055 309	0.000 004
74	6847.8899	0.0021	0.053 256	0.000 006
75	6885.2949	0.0011	0.051 115	0.000 004
76	6920.2664	0.0020	0.048 890	0.000 007
77	6952.7459	0.0011	0.046 607	0.000 004
78	6982.6934	0.0014	0.044 215	0.000 006
79	7010.0743	0.0011	0.041 732	0.000 003
80	7034.8772	0.0039	0.039 149	0.000 015
81	7057.0784	0.0038	0.036 529	0.000 016
82	7076.7146	0.0042	0.033 815	0.000 018
83	7093.3463	0.0109	0.029 442	0.000 027
84	7108.0794	0.0132	0.026 841	0.000 032
85	7120.9058	0.0037	0.025 516	0.000 011
86	7131.1525	0.0031	0.022 806	0.000 009
87	7139.4590	0.0034	0.020 178	0.000 012
88	7146.0513	0.0034	0.017 666	0.000 012
89	7151.1697	0.0032	0.015 275	0.000 009
90	7155.0296	0.0042	0.013 022	0.000 012
91	7157.8559	0.0045	0.010 895	0.000 017
92	7159.7977	0.0061	0.009 278	0.000 031
93	7161.1151	0.0056	0.007 150	0.000 064
94	7161.8810	0.0040	0.004 920	0.000 102
95	7162.2892	0.0025	0.003 580	0.000 080

To test the quality of the RKR potential, eigenvalues obtained from the RKR potential by solving the radial Schrödinger equation with the EIGEN code[64] are compared with the experimentally observed term values. The differences are about 0.1 cm^{-1} or less in most cases. Noticeably larger deviations (about 0.5 cm^{-1}) occur for $v=83$ and 84, where perturbations are present as indicated in Fig. 5.

Finally, D_e, T_e, ω_e, and R_e of the $1\,^3\Delta_g$ state of Na_2 determined by the NDE algorithm (with $Y_{00}^{(2)}$ correction included) are listed together in Table I, along with the primary molecular constants determined by other means in the foregoing discussions. The excellent agreement between these completely different and independent approaches is particularly gratifying and reassuring and demonstrates the ability of the NDE fits to represent the large data set from near dissociation levels all the way down to near equilibrium levels.

V. LONG-RANGE ANALYSIS OF THE $1\,^3\Delta_g$ STATE OF Na_2

A. Some general considerations

The highest observed vibrational level ($v=95$) has a rotationless binding energy of about 0.14 cm^{-1}. Since the spin–orbit splitting of Na($3d$) atom is only 0.049 cm^{-1}, spin–orbit interactions can be reasonably neglected in the long-range analysis of the observed near dissociation levels reported here. Therefore the spin–orbit-averaged Na($3s$) +Na($3d$) asymptote is taken as the dissociation limit in the determination of T_e or D_e. This is supported by the experimental observation that the fine–hyperfine structure remains the typical Hund's case ($b_{\beta S}$) coupling for the highest vibrational levels observed, such as shown in Fig. 2. In fact, the theoretical long-range calculation[9] for the Na($3s$)+Na($3d$) asymptote also neglected the spin–orbit interactions.

Before we proceed with the analysis, we must first determine the region of validity of the inverse-power expansion in the long range:

$$V(R)=D-\sum_{m\geqslant n}\frac{C_m}{R^m}. \tag{15}$$

For the $1\,^3\Delta_g$ state of Na_2, we have $n=5$ as the leading term, which comes from the quadrupole resonance between the Na($3s$) and Na($3d$) atoms; and it is followed by the dispersion terms $m=6,8,10$ etc. (see Ref. 43).

Traditionally, the Le Roy radius[43,65] $R_{\rm LR}$ has been widely used as the lower bound for Eq. (15) to be valid for pairs of atoms in s states:

$$R_{\rm LR}=2[\langle r^2\rangle_A^{1/2}+\langle r^2\rangle_B^{1/2}], \tag{16}$$

where $\langle r^2\rangle^{1/2}$ is the r.m.s. distance of the outermost electron (i.e., the valence electron) in the atom. For Na($3s$)+Na($3d$), we have $R_{\rm LR}=16.5$ Å.

More recently, a modified criteria, $R_{\text{LR-}m}$, which explicitly takes into account the spatial orientation of the atomic orbitals, has been proposed and shown to be an appropriate generalization of $R_{\rm LR}$ to pairs of atoms with non-s state involved:[66]

$$R_{\text{LR-}m}=2\sqrt{3}[\langle nlm|z^2|nlm\rangle_A^{1/2} +\langle n'l'm'|z^2|n'l'm'\rangle_B^{1/2}], \tag{17}$$

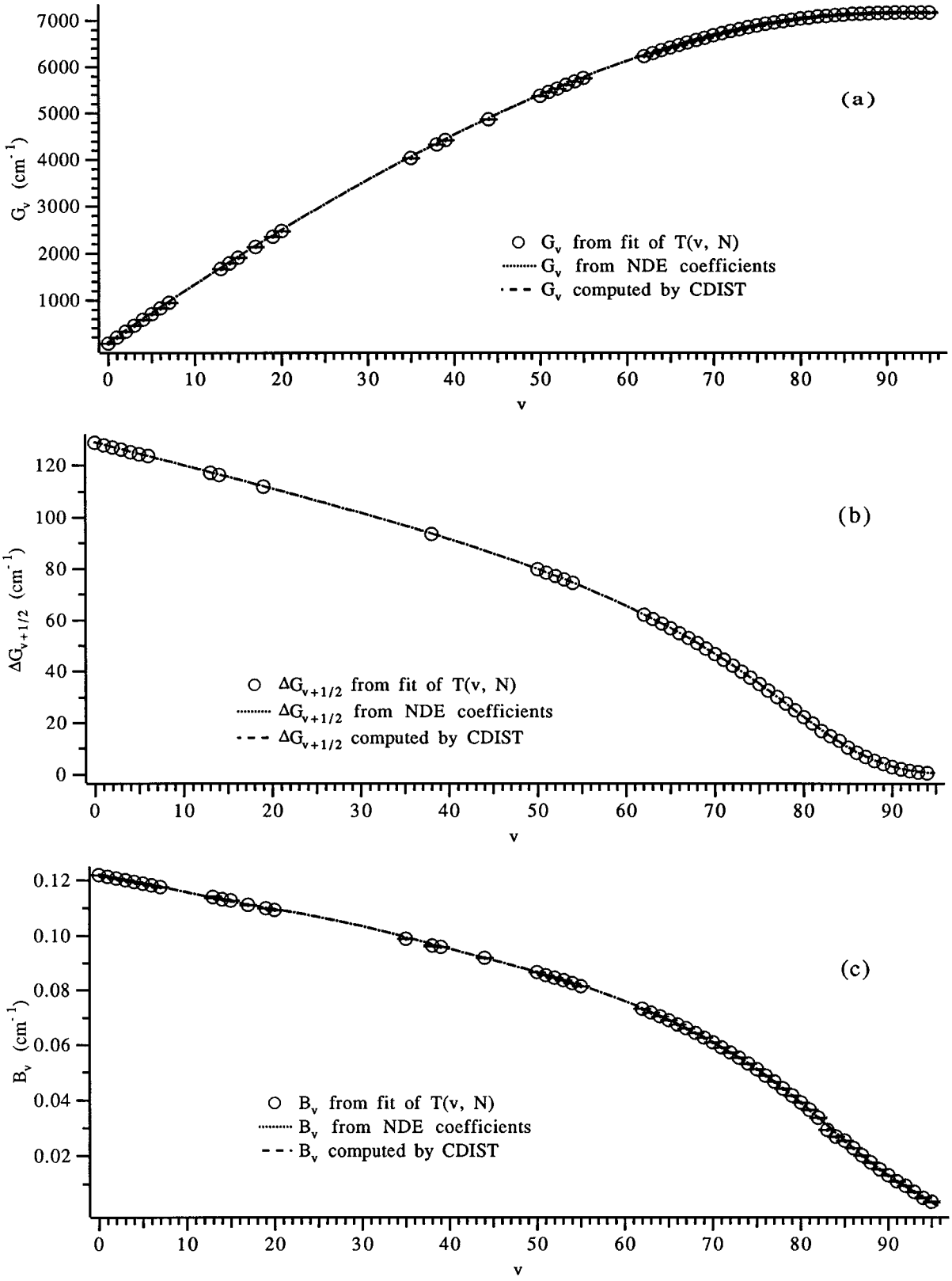

FIG. 5. Primary molecular constants of the $1\,^3\Delta_g$ state of Na_2 as a function of the vibrational quantum number v. (a) Vibrational energy G_v vs v. (b) $\Delta G_{v+1/2}$ vs v. (c) Rotational constant B_v vs v. The small horizontal bars in (a) and (c) are error bars representing the 1σ uncertainties from the least-squares fit of the experimental term values. In all three plots, the curves calculated from the fitted NDE coefficients (taken from Tables III and IV) overlap completely with the curves computed by the CDIST code (based on the RKR potential in Table V).

TABLE III. Parameters in the $(NP=0/NQ=15)$ inner Padé GvNDE fit of the $1\,^3\Delta_g$ state of Na_2.

Parameter	Recommended value	During fit
$LPWDV$	1	fixed
$NDP1$	2	fixed
$NDQ1$	2	fixed
$10^{-6}C_5$ (cm^{-1} Å^5)	0.792 281 77	fixed
$X_0(5)$ (cm^{-1})	0.018 294 384	fixed
v_D	96.884 825 62±0.049	variable
D_e (cm^{-1})	7162.436[a]±0.021	variable
$10q_1$	0.123 667 090 556	variable
10^2q_2	−0.266 806 293 657	variable
10^3q_3	0.286 774 876 597	variable
10^4q_4	−0.193 388 922 357	variable
10^6q_5	0.901 767 702 744	variable
10^7q_6	−0.305 503 033 758	variable
10^9q_7	0.772 290 708 653	variable
$10^{10}q_8$	−0.147 605 647 135	variable
$10^{12}q_9$	0.213 985 861 088	variable
$10^{14}q_{10}$	−0.233 925 577 848	variable
$10^{16}q_{11}$	0.189 713 705 325	variable
$10^{18}q_{12}$	−0.110 655 782 284	variable
$10^{21}q_{13}$	0.438 794 982 949	variable
$10^{23}q_{14}$	−0.105 896 461 424	variable
$10^{26}q_{15}$	0.117 371 319 830	variable

[a]The second-order correction $Y_{00}^{(2)}=0.0557$ cm^{-1} has been included.

where n and n' are the principal quantum numbers; l and l' are quantum numbers of the atomic electronic angular momentum; and m and m' are the components of $\mathbf{l}$ and $\mathbf{l}'$ on the internuclear axis $\hat{\mathbf{z}}$ for the outermost electrons in atoms A and B, respectively. Note that the angular dependence in $z=r\cos\theta$ reflects the separation of the two atoms along the internuclear axis. For the $1\,^3\Delta_g$ state of Na_2, we have $R_{\text{LR-}m}=12.43$ Å. This roughly corresponds to the outer turning point of $v=88$ level. In the following analysis, only $v\geqslant 85$ levels (corresponding to $R_+\geqslant 10.6$ Å) are considered in the long-range fits. This choice of long-range levels is corroborated by the observation that the inflection point (i.e., zero of the second derivative) for $\Delta G_{v+1/2}$ is around $v=80$ in Fig. 5(b) and and that the inflection point for B_v is around $v=84$ in Fig. 5(c), since these inflection points also indicate the ''onset'' of the long-range behavior.

TABLE IV. Parameters in the exponential BvNDE fit of the $1\,^3\Delta_g$ state of Na_2.

Parameter	Recommended value	During fit
$10^{-6}C_5$ (cm^{-1} Å^5)	0.792 281 77	fixed
$10^2X_1(5)$ (cm^{-1})	0.235 05	fixed
v_D	96.884 825 62	fixed
p_1	−0.294 701 23	variable
$10p_2$	0.398 617 45	variable
10^2p_3	−0.291 590 17	variable
10^3p_4	0.126 422 62	variable
10^5p_5	−0.348 724 41	variable
10^7p_6	0.628 701 7	variable
10^9p_7	−0.737 784	variable
$10^{11}p_8$	0.542 66	variable
$10^{13}p_9$	−0.227 03	variable
$10^{16}p_{10}$	0.412	variable

Various fitting schemes have been employed to determine the long-range coefficients C_m's from spectroscopic data in the literature.[27,56,67–70] Here we present the results of two different approaches.

B. Fitting of the potential turning points

Once the reliable RKR potential curve is constructed, outer turning points of $v=85$–95 levels are graphically examined in Fig. 7 according to the linear relation:

$$[V(R)-D_e]R^6=-C_5R-C_6. \tag{18}$$

It is apparent in Fig. 7 that the outer turning points of $v=88$–92 levels conform to Eq. (18) so these turning points are used in the linear least squares fit to extract the C_5 and C_6 coefficients, which are listed in Table VI.

C. Direct determination from the spectroscopic data

Le Roy and co-workers[69] have developed an algorithm which extracts the long-range coefficients C_m's directly from the spectroscopic data. Compared with the turning point fitting method, it can directly take into account the effect of uncertainties in the experimental data. Interparameter correlation is also reduced in this direct fitting procedure. Based on JWKB quantization condition of diatomic molecule in the long-range potential given by Eq. (15), the coefficients C_m's can be determined by fitting G_v's and B_v's into

$$B_v=\frac{I_2}{\beta^2 I_0}, \tag{19}$$

where $\beta=(2\mu/\hbar^2)$, μ is the reduced mass of the molecule, and I_l is given by

$$I_l=\int_0^{R_+}R^{-l}\left[\sum_{m\geqslant n}\frac{C_m}{R^m}-(D-G_v)\right]^{-1/2}dR, \tag{20}$$

and

$$v=v_D-\left(\frac{\beta}{\pi}\right)\int_0^{R_+}\left\{\left[\sum_{m\geqslant n}\frac{C_m}{R^m}\right]^{1/2}-\left[\sum_{m\geqslant n}\frac{C_m}{R^m}-(D-G_v)\right]^{1/2}\right\}dR-\left(\frac{\beta}{\pi}\right)\int_{R_+}^{\infty}\left[\sum_{m\geqslant n}\frac{C_m}{R^m}\right]^{1/2}dR. \tag{21}$$

A computer code (CmDFIT)[70] is used to carry out the nonlinear least-squares fit. G_v and B_v values as well as their associated uncertainties for $85\leqslant v\leqslant 95$ in Table II are taken as the input. To address the issue of model dependence (such as dependence on data sets with different sizes), the ''averaging-over-models'' procedure as described in Refs. 14 and 69 is adopted here to generate the final C_m values and their uncertainties listed in Table VI. While higher-order terms (such as C_{10} and C_{12}) help to damp the fluctuations of the lower-order coefficients during the fits, they tend to have unreasonably large uncertainties themselves, possibly due to interparameter correlation with the truncated (even higher-order) terms. Since all the $m\geqslant 10$ terms make negligible contributions to the potential of interest, these higher-order coefficients are not listed in Table VI. This choice of truncation

TABLE V. RKR potential of the $1\,^3\Delta_g$ state of Na_2. R_e=3.463 809 Å.

v	G_v (cm^{-1})	dG_v/dv (cm^{-1})	B_v (cm^{-1})	R_- (Å)	R_+ (Å)
0	64.6948	129.0846	0.121 852 04	3.319 947	3.621 485
1	193.3585	128.2285	0.121 186 71	3.222 050	3.745 592
2	321.1379	127.3283	0.120 586 44	3.157 494	3.835 314
3	448.0159	126.4293	0.120 003 16	3.106 633	3.910 988
4	574.0004	125.5414	0.119 409 10	3.063 900	3.978 627
5	699.1014	124.6614	0.118 791 06	3.026 777	4.041 006
6	823.3238	123.7833	0.118 145 97	2.993 849	4.099 668
7	946.6673	122.9031	0.117 477 20	2.964 203	4.155 553
8	1069.1286	122.0190	0.116 791 84	2.937 198	4.209 271
9	1190.7042	121.1317	0.116 098 60	2.912 357	4.261 224
10	1311.3914	120.2425	0.115 406 26	2.889 304	4.311 695
11	1431.1893	119.3532	0.114 722 69	2.867 743	4.360 880
12	1550.0981	118.4646	0.114 054 15	2.847 432	4.408 932
13	1668.1189	117.5771	0.113 405 00	2.828 176	4.455 964
14	1785.2525	116.6900	0.112 777 55	2.809 816	4.502 078
15	1901.4987	115.8023	0.112 172 20	2.792 224	4.547 362
16	2016.8564	114.9125	0.111 587 55	2.775 299	4.591 900
17	2131.3225	114.0192	0.111 020 75	2.758 962	4.635 774
18	2244.8933	113.1214	0.110 467 75	2.743 154	4.679 064
19	2357.5635	112.2182	0.109 923 68	2.727 831	4.721 850
20	2469.3279	111.3095	0.109 383 19	2.712 966	4.746 211
21	2580.1807	110.3952	0.108 840 74	2.698 539	4.806 223
22	2690.1166	109.4758	0.108 290 93	2.684 541	4.847 958
23	2799.1307	108.5516	0.107 728 71	2.670 969	4.889 486
24	2907.2185	107.6232	0.107 149 64	2.657 822	4.930 873
25	3014.3759	106.6909	0.106 550 04	2.645 103	4.972 180
26	3120.5991	105.7547	0.105 927 06	2.632 813	5.013 463
27	3225.8840	104.8145	0.105 278 82	2.620 954	5.054 776
28	3330.2264	103.8695	0.104 604 35	2.609 524	5.096 164
29	3433.6213	102.9192	0.103 903 60	2.598 518	5.137 672
30	3536.0626	101.9623	0.103 177 36	2.587 930	5.179 337
31	3637.5433	100.9978	0.102 427 17	2.577 746	5.221 195
32	3738.0553	100.0246	0.101 655 16	2.567 953	5.263 276
33	3837.5892	99.0415	0.100 863 93	2.558 531	5.305 607
34	3936.1346	98.0475	0.100 056 38	2.549 461	5.348 212
35	4033.6803	97.0419	0.099 235 57	2.540 720	5.391 111
36	4130.2143	96.0240	0.098 404 52	2.532 283	5.434 324
37	4225.7241	94.9935	0.097 566 09	2.524 126	5.477 865
38	4320.1970	93.9501	0.096 722 86	2.516 224	5.521 752
39	4413.6199	92.8934	0.095 876 98	2.508 554	5.565 999
40	4505.9794	91.8234	0.095 030 09	2.501 092	5.610 623
41	4597.2622	90.7397	0.094 183 27	2.493 818	5.655 640
42	4687.4542	89.6420	0.093 336 97	2.486 713	5.701 073
43	4776.5412	88.5295	0.092 490 98	2.479 760	5.746 946
44	4864.5081	87.4015	0.091 644 47	2.472 946	5.793 288
45	4951.3388	86.2569	0.090 795 99	2.466 257	5.840 135
46	5037.0160	85.0945	0.089 943 52	2.459 687	5.887 529
47	5121.5213	83.9126	0.089 084 53	2.453 228	5.935 518
48	5204.8343	82.7098	0.088 216 09	2.446 878	5.984 159
49	5286.9334	81.4844	0.087 334 93	2.440 636	6.033 516
50	5367.7951	80.2348	0.086 437 58	2.434 503	6.083 658
51	5447.3943	78.9592	0.085 520 44	2.428 483	6.134 664
52	5525.7043	77.6562	0.084 579 93	2.422 583	6.186 620
53	5602.6970	76.3243	0.083 612 55	2.416 808	6.239 618
54	5678.3427	74.9621	0.082 615 01	2.411 166	6.293 757
55	5752.6107	73.5684	0.081 584 30	2.405 667	6.349 142
56	5825.4686	72.1418	0.080 517 75	2.400 319	6.405 889
57	5896.8829	70.6810	0.079 413 06	2.395 129	6.464 121
58	5966.8187	69.1844	0.078 268 31	2.390 105	6.523 970
59	6035.2392	67.6502	0.077 081 94	2.385 252	6.585 581
60	6102.1059	66.0765	0.075 852 74	2.380 572	6.649 115
61	6167.3783	64.4610	0.074 579 71	2.376 068	6.714 748
62	6231.0132	62.8012	0.073 262 01	2.371 737	6.782 678
63	6292.9651	61.0945	0.071 898 82	2.367 577	6.853 126
64	6353.1856	59.3380	0.070 489 16	2.363 581	6.926 345
65	6411.6237	57.5292	0.069 031 82	2.359 743	7.022 617
66	6468.2256	55.6654	0.067 525 15	2.356 061	7.082 274
67	6522.9354	53.7445	0.065 966 92	2.352 535	7.165 694
68	6575.6949	51.7645	0.064 354 28	2.349 166	7.253 305
69	6626.4444	49.7243	0.062 683 61	2.345 952	7.345 600
70	6675.1231	47.6229	0.060 950 55	2.342 894	7.443 144
71	6721.6695	45.4598	0.059 150 07	2.339 993	7.546 592
72	6766.0221	43.2352	0.057 276 58	2.337 248	7.656 711
73	6808.1195	40.9494	0.055 324 21	2.334 661	7.774 404
74	6847.9008	38.6034	0.053 287 16	2.332 232	7.900 749
75	6885.3069	36.1991	0.051 160 17	2.329 962	8.037 046
76	6920.2805	33.7393	0.048 939 15	2.327 852	8.184 872
77	6952.7686	31.2290	0.046 621 81	2.325 902	8.346 153
78	6982.7244	28.6761	0.044 208 46	2.324 113	8.523 255
79	7010.1106	26.0926	0.041 702 74	2.322 484	8.719 088
80	7034.9049	23.4953	0.039 112 31	2.321 015	8.937 238
81	7057.1043	20.9073	0.036 449 37	2.319 705	9.182 127
82	7076.7320	18.3573	0.033 730 95	2.318 551	9.459 217
83	7093.8428	15.8795	0.030 978 76	2.317 547	9.775 263
84	7108.5274	13.5111	0.028 218 71	2.316 687	10.138 660
85	7120.9142	11.2900	0.025 479 73	2.315 964	10.559 899
86	7131.1680	9.2505	0.022 792 29	2.315 366	11.052 217
87	7139.4850	7.4202	0.020 186 29	2.314 882	11.632 564
88	7146.0840	5.8164	0.017 688 67	2.314 498	12.323 099
89	7151.1954	4.4449	0.015 320 74	2.314 201	13.153 724
90	7155.0491	3.2991	0.013 095 41	2.313 977	14.166 764
91	7157.8633	2.3622	0.011 014 17	2.313 814	15.426 502
92	7159.8352	1.6102	0.009 063 76	2.313 699	17.040 780
93	7161.1365	1.0167	0.007 212 02	2.313 624	19.216 031
94	7161.9140	0.5599	0.005 402 77	2.313 579	22.421 201
95	7162.2990	0.2321	0.003 553 32	2.313 557	28.021 329
96	7162.4246	0.0440	0.001 584 04	2.313 549	42.534 364

of the higher-order dispersion terms can be corroborated by a simple estimation based on the recursion relation

$$C_{m+4} = \gamma \frac{C_{m+2}^2}{C_m}, \tag{22}$$

where γ is a dimensionless constant of the order of unity.[42,65,71–73]

D. Discussion

Table VI also lists the recent theoretical calculations of C_5 and C_6 values by Bussery and Fréon[9] and Marinescu and Dalgarno.[10] They agree reasonably well with our experimental values extracted by two different approaches. All four sets of long-range coefficients are graphically examined in Fig. 7, where the quantitative differences among them have been dramatically magnified by the factor R^6. While the four sets of C_m's do not overlap one another in Fig. 7, Fig. 8(a) demonstrates that all of them can provide satisfactory representation of the long-range potential of the $1\,^3\Delta_g$ state of Na_2. The apparently large discrepancy of the C_5 values determined in this work is mainly due to the interparameter correlation in the fit. This numerical deficiency is aggravated by the fact that the long-range potential is overwhelmingly dominated by the C_6 term for all the bound levels used in the fit, as shown in Fig. 8(b). It is also apparent from Fig. 8(b) that the contribution from the C_8 term is insignificant.

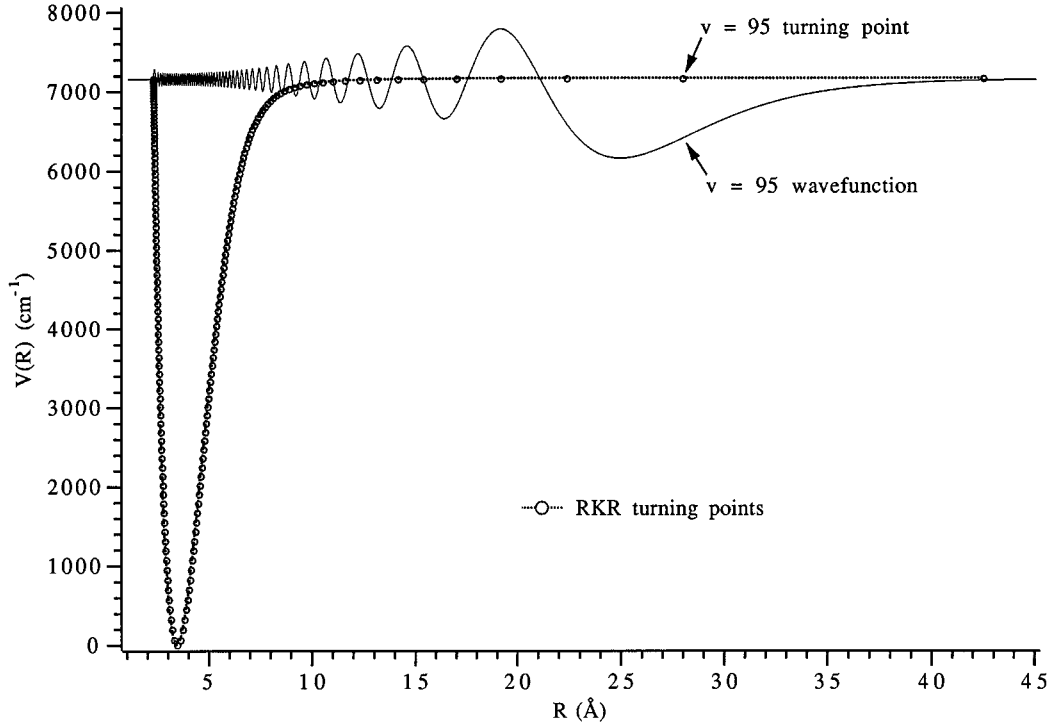

FIG. 6. RKR potential curve of the $1\,^3\Delta_g$ state of Na_2 and the wave function of the ($v=95$, $N=2$) level.

It might appear to be paradoxical that a reasonably high quality RKR potential could be constructed with the constraints on C_5 alone in Sec. IV C, despite the fact that the C_6 term actually contributes much more to the potential than the C_5 term even at the outermost observed turning point ($v=95$, or $R_+=28.02$ Å). This can be understood first by noting that the limiting form of G_v in Eqs. (6) and (8) has a power of 3 for $n=6$, which is quite close to the power of 10/3 for $n=5$. In addition, there is a fortuitous, *but not accidental*, cancellation of deviations from the limiting behavior by the $m \geqslant n$ higher-order terms. In general, when the second inverse-power term in Eq. (15) has $m=n+1$, the leading correction

TABLE VI. Long-range coefficients of the $1\,^3\Delta_g$ state of Na_2.

	Bussery & Aubert-Frécon[a,b]	Marinescu & Dalgarno[a,c]	RKR turning point fit, this work[a,d,e]	Averaged G_v & B_v fit, this work[a,e,f]
$10^{-6}C_5$ (cm^{-1} Å^5)	0.792	0.8778	1.388 (0.031)	0.23 (0.12)
$10^{-8}C_6$ (cm^{-1} Å^6)	0.522 041	0.498 76	0.4008 (0.0046)	0.557 (0.040)
$10^{-8}C_8$ (cm^{-1} Å^8)				0.49 (0.32×10^6)

[a]Sign convention: positive values are attractive.
[b]From Ref. 9.
[c]From Ref. 10.
[d]Based on least squares fit of $88 \leqslant v \leqslant 92$ RKR turning points.
[e]1σ uncertainties are in parentheses.
[f]Based on "averaging-over-models" fit of G_v and B_v for $85 \leqslant v \leqslant 95$.

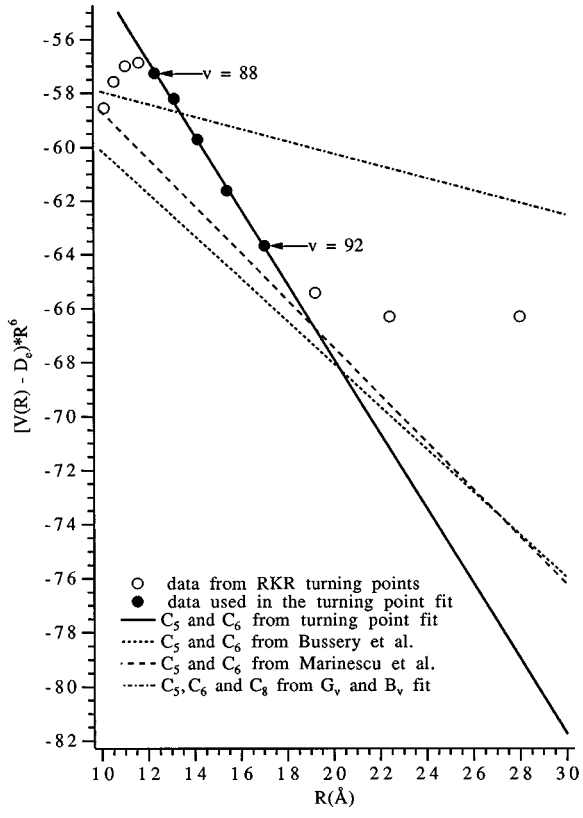

FIG. 7. Turning point fitting of the long-range coefficients of the $1\,^3\Delta_g$ state of Na_2. Other sets of long-range coefficients are also examined in the plot.

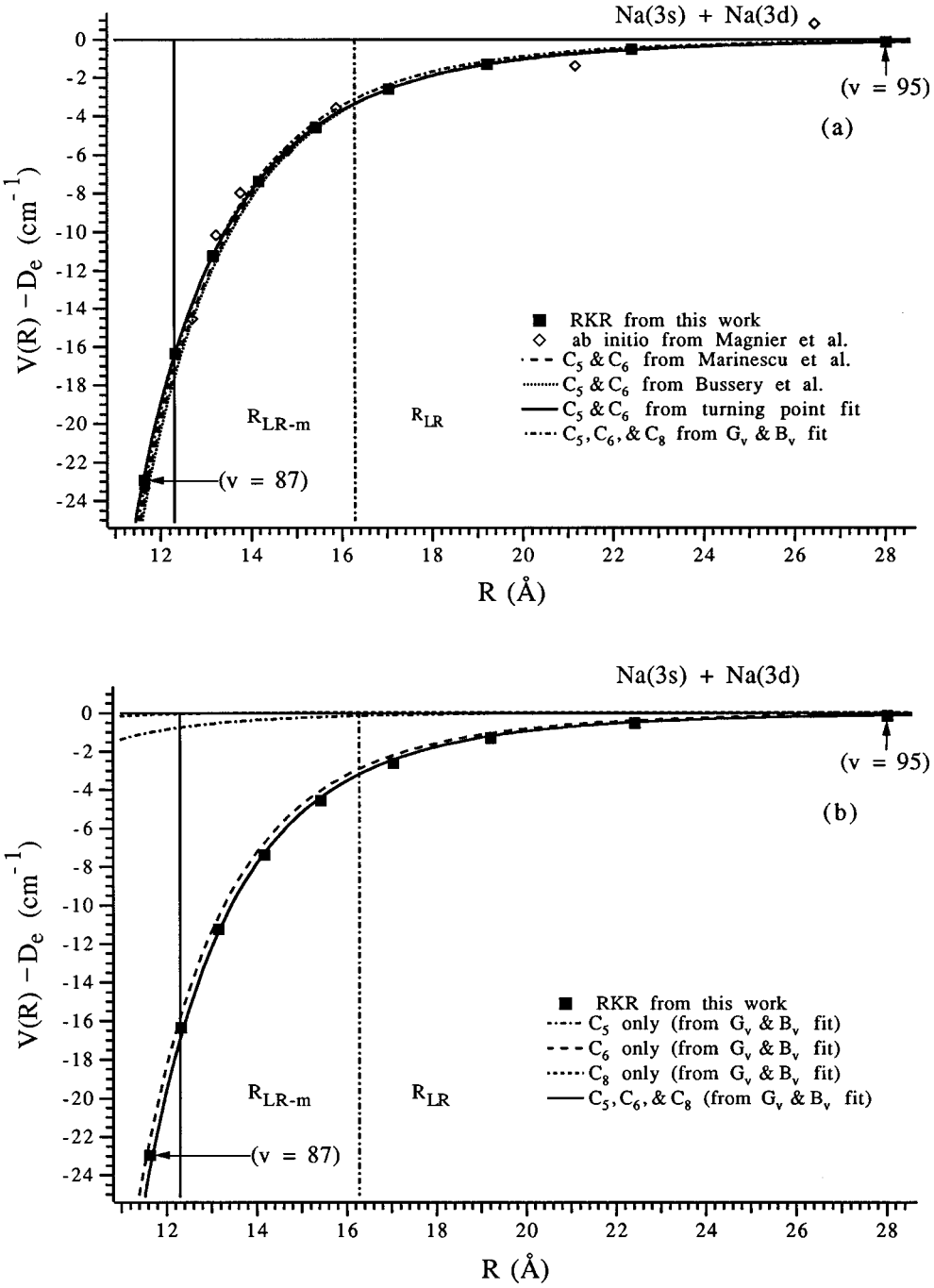

FIG. 8. The long-range potential of the $1\,^3\Delta_g$ state of Na_2. (a) Comparison of the potential curves determined by various means. (b) Comparison of the C_5, C_6, and C_8 contributions to the long-range potential. The C_m's in the plot are taken from the direct fitting of the long-range region G_v's and B_v's.

to the one term C_n limiting expression for level energies is identically zero. This issue has been quantitatively addressed in detail in Ref. 42. In passing we note that a very similar case occurs in the A state of I_2.[74]

E. Properties of the $1\,^3\Delta_g$ state at long range

The highest observed vibrational level ($v=95$) has a binding energy of only 0.14 cm^{-1} and an outer turning point of 28.02 Å, i.e., about $8R_e$. It has long been pointed out that molecules at such long range will exhibit some unique or even exotic properties that are not seen in the normal deeply bound levels.[35,36,75] Thus, molecules in such a long-range state are often referred to as long-range molecules. To understand this in the picture of quantum mechanics, the rotationless vibrational wave function of the ($v=95$, $N=2$) level is plotted in Fig. 6. It is apparent that the molecule spends most of its vibration period around the outer turning point. In fact, the molecule has a much larger probability to be outside the outer wall of the potential than that to be near the inner wall, even though the former is classically forbidden. A direct consequence of this ''exotic'' wave function is that the transition probability for the PROBE step diminishes exponentially as

v approaches v_D. Quantitative calculation gives the Franck–Condon factor (FCF) for the highest observed PROBE transition, $1\,^3\Delta_g(v=95)\leftarrow b\,^3\Pi_u(v'=25)$, to be 3.5×10^{-6} (normalized to 1.0), which is about five orders of magnitude smaller than FCF$=1.435\times10^{-1}$ for one of the strongest transitions observed in the experiment $[1\,^3\Delta_g(v=14)\leftarrow b\,^3\Pi_u(v'=25)]$. This is the obvious reason that these long-range molecules are extremely difficult to access by conventional spectroscopic approaches and have rarely been observed experimentally until recently. In passing we note that the transition to the extrapolated level $[1\,^3\Delta_g(v=96)\leftarrow b\,^3\Pi_u(v'=25)]$ has a FCF of 3.4×10^{-7}. Despite the efforts that had been attempted, the sensitivity of the experimental setup was not enough to detect such weak signals.

The low kinetic energy and high density of states of the long-range molecules lead to some unusual aspects in radiative, nonradiative, and collision-induced transitions involving long-range levels.[38,39,75] For radiative electronic transitions, the Franck–Condon principle requires that the most favorable transitions are limited to those between two long-range levels with similar outer turning points in the upper and lower states. In addition, the atomic asymptotes of the upper and the lower electronic states must have electric dipole allowed transitions between them for the transitions between the upper and the lower long-range levels to be favorable. This unique property has been ingeniously utilized by photoassociative spectroscopy techniques to observe long-range molecules in recent years.[76–78] Such highly selective electronic transitions, however, lead to weaker UV/violet fluorescence which is pivotal to the filtered PMT detection method described earlier in Sec. II. This is because electric dipole transitions are not allowed between the $Na(3s)+Na(3d)$ and $Na(3s)+Na(3s)$ asymptotes. On the other hand, the extremely long vibrational period and large internuclear separation give rise to greatly enhanced cross sections for collisional ionization processes,[12] such as associative ionization, $Na_2^* + Na \rightarrow Na_3^+ + e^-$. The cylindrically shielded ionization detector takes advantage of this long-range property and thus enables us to observe these extremely weak PROBE transitions in the OODR spectroscopy. This has allowed us to construct an extensive experimental potential curve over 99.998% of the well depth.

Before closing the discussions here, we point out an intriguing or even provocative speculation: the ''averaging-over-models'' value of v_D in Sec. IV C is 96.80 ± 0.20. One might thus contemplate the possible existence of such an extremely weakly bound $v=97$ level. It must be noted, however, that the v_D parameter in the present model is an effective value corresponding to the spin–orbit-averaged atomic asymptote. This approximated asymptote is obviously inadequate to study the very last few weakly bound levels. More extensive studies which explicitly treat the spin–orbit and hyperfine interactions are clearly called for in the analysis of the $v=96$ and possibly $v=97$ levels. One might hope that novel spectroscopic methods, such as photoassociative spectroscopy, may be able to observe these very last bound levels of the $1\,^3\Delta_g$ state of Na_2 along with other long-range states that dissociate into the same asymptote and depict a more complete picture of these fundamental interactions (such as exchange interaction at moderately long range, and recoupling of angular momenta at very long range, or even retardation effects at extremely long range). Furthermore, the potential curves provided by these studies would pave the way for the study of state-selected ultracold photodissociation of purely attractive long-range molecules, where fine-structure changing and alignment effects are important aspects of the dynamical processes. While such detailed experimental study on the photodissociation dynamics is extremely difficult, it has been carried out in the NaK ($B\,^1\Pi\leftarrow X\,^1\Sigma^+$) system in a molecular beam.[79] State selectivity in photodissociation has been achieved in the study of the K_2 ($B\,^1\Pi_u\leftarrow X\,^1\Sigma_g^+$) system by all-optical triple resonance (AOTR) spectroscopy recently.[80,81] It remains a great challenge to carry out similar investigations into the $1\,^3\Delta_g$ state of Na_2 in the future.

VI. CONCLUSION

We have demonstrated that the cylindrically shielded ionization detector can provide the high sensitivity for observation of long-range molecules in OODR spectroscopy. Our analysis of the $1\,^3\Delta_g$ state of Na_2 shows that the near dissociation expansion (NDE) theory is a more versatile and physically reliable approach both in data representation and in potential inversion. The observed rovibrational levels in the $1\,^3\Delta_g$ state of Na_2 have covered over 99.998% of the potential well depth and exhibited significant long-range behavior. We hope that this work will pave the way for more investigations in the future, such as perturbation analysis between the $1\,^3\Delta_g$ state and other nearby electronic states of Na_2, as well as those mentioned in the last section. Furthermore, we hope that the success of the NDE analysis in this detailed case study may stimulate further interests of applying the NDE approach to spectral analysis as well as molecular dynamics studies of other molecular systems.

ACKNOWLEDGMENTS

We thank Professor F. Masnow-Seeuws and Professor A. Dalgarno for providing their results prior to publication, and Dr. Photos G. Hajigeorgiou and Ken Urbanski for their critical and helpful discussions. We also thank the referee for helpful comments and corrections. Financial support from the National Science Foundation is gratefully acknowledged.

[1] L. Li and R. W. Field, J. Mol. Spectrosc. **117**, 245 (1986).
[2] L. Li, Q. Zhu, and R. W. Field, J. Mol. Spectrosc. **134**, 50 (1989).
[3] L. Li, A. M. Lyyra, and W. C. Stwalley, J. Mol. Spectrosc. **134**, 113 (1989).
[4] L. Li, A. M. Lyyra, W. C. Stwalley, M. Li, and R. W. Field, J. Mol. Spectrosc. **147**, 215 (1991).
[5] G. H. Jeung, Phys. Rev. A **35**, 26 (1987).
[6] A. Henriet and F. Masnou-Seeuws, J. Phys. B **20**, 671 (1987).
[7] S. Magnier, Ph. Millié, O. Dulieu, and F. Masnou-Seeuws, J. Chem. Phys. **98**, 7113 (1993).
[8] S. Magnier, Ph.D. Thesis, University de Paris-SUD, Centre D'Orsay, France (1993).
[9] B. Bussery and M. Aubert-Frécon, J. Mol. Spectrosc. **115**, 169 (1986).
[10] M. Marinescu and A. Dalgarno, Phys. Rev. A **52**, 311 (1995).
[11] J. Tellinghuisen, J. Chem. Phys. **78**, 2374 (1983).
[12] C.-C. Tsai, J. T. Bahns, and W. C. Stwalley, Rev. Sci. Instrum. **63**, 5575 (1992).
[13] J. W. Tromp and R. J. Le Roy, J. Mol. Spectrosc. **109**, 352 (1985).

[14] K. J. Jordan, R. H. Lipson, N. A. McDonald, and R. J. Le Roy, J. Phys. Chem. **96**, 4778 (1992).
[15] C.-C. Tsai, J. T. Bahns, H. Wang, W. C. Stwalley, and A. M. Lyyra, Phys. Rev. Lett. **71**, 1152 (1993).
[16] C.-C. Tsai, J. T. Bahns, and W. C. Stwalley, J. Chem. Phys. **99**, 7417 (1993).
[17] C.-C. Tsai, J. T. Bahns, and W. C. Stwalley, J. Chem. Phys. **99**, 8480 (1993).
[18] C.-C. Tsai, J. T. Bahns, and W. C. Stwalley, J. Chem. Phys. **100**, 768 (1994).
[19] C.-C. Tsai, J. T. Bahns, H. Wang, T.-J. Whang, and W. C. Stwalley, J. Chem. Phys. **101**, 25 (1994).
[20] C.-C. Tsai, J. T. Bahns, and W. C. Stwalley, J. Mol. Spectrosc. **167**, 429 (1994).
[21] C.-C. Tsai, J. T. Bahns, T.-J. Whang, and W. C. Stwalley, J. Mol. Spectrosc. **167**, 437 (1994).
[22] J. B. Atkinson, J. Becker, and W. Demtröder, Chem. Phys. Lett. **87**, 128 (1982).
[23] H. Knöckel, T. Johr, H. Richter, and E. Tiemann, Chem. Phys. **152**, 399 (1991).
[24] W. T. Zemke and W. C. Stwalley, J. Chem. Phys. **100**, 2661 (1994).
[25] G. Herzberg, *Molecular Spectra and Molecular Structure, Vol. 1, Spectra of Diatomic Molecules*, 2nd ed. (Krieger, Malabar, FL, 1989).
[26] W. M. Kosman and J. Hinze, J. Mol. Spectrosc. **56**, 93 (1975).
[27] C. R. Vidal and H. Scheingraber, J. Mol. Spectrosc. **65**, 46 (1977).
[28] H. Richter, H. Knöckel, and E. Tiemann, Chem. Phys. **157**, 217 (1991).
[29] W. C. Stwalley, in *Energy, Structure and Reactivity*, edited by D. W. Smith and W. B. McRae (Wiley, New York, 1973), p. 259.
[30] W. C. Stwalley, J. Chem. Phys. **63**, 3062 (1975).
[31] J. L. Dunham, Phys. Rev. **41**, 713 (1932); **41**, 726 (1932).
[32] C. L. Beckel and R. Engelke, J. Chem. Phys. **49**, 5199 (1968).
[33] G. Simons, R. G. Parr, and J. M. Finlan, J. Chem. Phys. **59**, 3229 (1973).
[34] R. J. Le Roy and R. B. Bernstein, Chem. Phys. Lett. **5**, 42 (1970).
[35] R. J. Le Roy and R. B. Bernstein, J. Chem. Phys. **52**, 3869 (1970).
[36] W. C. Stwalley, Chem. Phys. Lett. **6**, 241 (1970).
[37] W. C. Stwalley, J. Chem. Phys. **58**, 3867 (1973).
[38] W. C. Stwalley, Contemp. Phys. **19**, 65 (1978).
[39] W. C. Stwalley, Y.-H. Uang, and G. Pichler, Phys. Rev. Lett. **41**, 1164 (1978).
[40] R. J. Le Roy, Can. J. Phys. **50**, 953 (1972).
[41] R. J. Le Roy, in *Semiclassical Methods in Molecular Scattering and Spectroscopy*, edited by M. S. Child (Reidel, Dordrecht, The Netherlands, 1980), p. 109.
[42] R. J. Le Roy, J. Chem. Phys. **73**, 6003 (1980).
[43] R. J. Le Roy, in *Molecular Spectroscopy*, edited by R. F. Barrow, D. A. Long, and D. J. Millen (Chemical Society, London, 1973), p. 113.
[44] A.-R. Hashemi-Attar, C. L. Beckel, W. N. Keepin, and S. A. Sonnleitner, J. Chem. Phys. **70**, 3881 (1979).
[45] A.-R. Hashemi-Attar and C. L. Beckel, J. Chem. Phys. **71**, 4596 (1979).
[46] C. L. Beckel and R. B. Kwong, J. Chem. Phys. **73**, 4698 (1980).
[47] C. L. Beckel, R. B. Kwong, A.-R. Hashemi-Attar, and R. J. Le Roy, J. Chem. Phys. **81**, 66 (1984).
[48] R. J. Le Roy and M. G. Barwell, Can. J. Phys. **53**, 1983 (1975).
[49] R. J. Le Roy and W.-H. Lam, Chem. Phys. Lett. **71**, 544 (1980).
[50] J. W. Tromp and R. J. Le Roy, Can. J. Phys. **60**, 26 (1982).
[51] G. A. Baker, Jr., *Essentials of Padé Approximants* (Academic, New York, 1975).
[52] G. A. Baker, Jr. and P. Graves-Morris, *Padé Approximants* (Addison-Wesley, Reading, MA, 1981).
[53] Programs *Gv*NDE and *Bv*NDE which perform the NDE fits may be obtained from R. J. Le Roy by sending a request via electronic mail to leroy@UWaterloo.ca.
[54] L. Li, S. F. Rice, and R. W. Field, J. Chem. Phys. **82**, 1178 (1985).
[55] E. J. Friedman-Hill and R. W. Field, J. Chem. Phys. **96**, 2444 (1992).
[56] C. Amiot, J. Chem. Phys. **93**, 8591 (1990).
[57] E. S. Hertel, Jr. and C. L. Beckel, Bull. Am. Phys. Soc. **24**, 447 (1979).
[58] R. J. Le Roy, *RKR1, A Computer Program Implementing the First-Order RKR Method for Determining Diatom Potential Energy Curves from Spectroscopic Constants* (University of Waterloo Report, 1992). Program RKR1 may be obtained from R. J. Le Roy by sending a request via electronic mail to leroy@UWaterloo.ca.
[59] W. C. Stwalley, J. Chem. Phys. **56**, 2485 (1972).
[60] J. M. Hutson, J. Phys. B **14**, 851 (1981).
[61] J. M. Hutson, S. Gerstenkorn, P. Luc, and J. Sinzelle, J. Mol. Spectrosc. **96**, 266 (1982).
[62] R. P. Verma, J. Chem. Phys. **32**, 738 (1960).
[63] B. H. Wells, E. B. Smith, and R. N. Zare, Chem. Phys. Lett. **99**, 244 (1988).
[64] K. M. Sando and A. Dalgarno, Mol. Phys. **20**, 103 (1971).
[65] R. J. Le Roy, Can. J. Phys. **52**, 246 (1974).
[66] B. Ji, C.-C. Tsai, and W. C. Stwalley, Chem. Phys. Lett. **236**, 242 (1995).
[67] W. C. Stwalley, Chem. Phys. Lett. **7**, 600 (1970).
[68] K. C. Li and W. C. Stwalley, J. Chem. Phys. **59**, 4423 (1973).
[69] M. R. Davis, J. C. Shelley, and R. J. Le Roy, J. Chem. Phys. **94**, 3479 (1991).
[70] Program CmDFIT which performs direct fit of long-range inverse power potential coefficients from spectroscopic data may be obtained from R. J. Le Roy by sending a request via electronic mail to leroy@UWaterloo.ca.
[71] T. R. Proctor and W. C. Stwalley, J. Chem. Phys. **66**, 2063 (1977).
[72] A. J. Thakkar and V. D. Smith, Chem. Phys. Lett. **17**, 274 (1972).
[73] A. J. Thakkar and V. D. Smith, J. Phys. B **7**, 1321 (1974).
[74] D. R. T. Appadoo, R. J. Le Roy, P. F. Bernath, S. Gerstenkorn, P. Luc, J. Vergés, J. Sinzelle, J. Chevillard, and Y. D'Aignaux, J. Chem. Phys. (submitted).
[75] W. C. Stwalley and W. T. Zemke, Int. J. Quantum Chem. **S10**, 223 (1976).
[76] H. R. Thorsheim, J. Weiner, and P. S. Julienne, Phys. Rev. Lett. **58**, 2420 (1987).
[77] J. D. Miller, R. A. Cline, and D. J. Heinzen, Phys. Rev. Lett. **71**, 2204 (1993).
[78] A. J. Moerdijk, W. C. Stwalley, R. C. Hulet, and B. J. Verhaar, Phys. Rev. Lett. **72**, 40 (1994).
[79] J. X. Wang, P. D. Kleiber, K. M. Sando, and W. C. Stwalley, Phys. Rev. A **42**, 5352 (1990).
[80] B. Ji, A. Yiannopoulou, P. D. Kleiber, A. M. Lyyra, and W. C. Stwalley, Phys. Rev. A **49**, R1535 (1994).
[81] B. Ji, P. D. Kleiber, W. C. Stwalley, A. Yiannopoulou, A. M. Lyyra, and P. S. Julienne, J. Chem. Phys. **102**, 2440 (1995).